metals

MDPI

Article

Cooling Rate Controlled Aging of a Co-Free Fe-Ni-Cr-Mo-Ti-Al Maraging Steel

Stefan Zeisl * and Ronald Schnitzer

Department of Materials Science, Montanuniversität Leoben, Franz-Josef Straße 18, 8700 Leoben, Austria; ronald.schnitzer@unileoben.ac.at

* Correspondence: stefan.zeisl@unileoben.ac.at

Abstract: Maraging steels are high-strength steels that are hardened by the formation of precipitates during an isothermal aging heat treatment. Depending on the aging temperature and time the cooling rate after holding can play a significant factor on the development of the microstructure and mechanical properties. This study seeks to show how the cooling time influences the precipitation hardening effect, austenite reversion and the development of hardness and impact toughness. The material was aged at a constant temperature using holding times of 0 h, 4 h and 15 h and cooled with different cooling rates resulting in cooling times of 7 h, 28 h and 56 h. The microstructure was characterized using a combination of electron backscatter diffraction, X-ray diffraction and atom probe tomography with cluster-based precipitate analysis. It is shown that the effect of the cooling time is strongly dependent on the holding time and that a longer cooling time can improve hardness and impact toughness.

Keywords: maraging steels; atom probe tomography; heat treatment study; X-ray diffraction; intermetallic precipitates

check for updates

Citation: Zeisl, S.; Schnitzer, R. Cooling Rate Controlled Aging of a Co-Free Fe-Ni-Cr-Mo-Ti-Al Maraging Steel. *Metals* **2022**, *12*, 538. https://doi.org/10.3390/met12040538

Academic Editor: Angelo Fernando Padilha

Received: 2 March 2022
Accepted: 18 March 2022
Published: 22 March 2022

Publisher's Note: MDPI stays neutral with regard to jurisdictional claims in published maps and institutional affiliations.

Copyright: © 2022 by the authors. Licensee MDPI, Basel, Switzerland. This article is an open access article distributed under the terms and conditions of the Creative Commons Attribution (CC BY) license (https://creativecommons.org/licenses/by/4.0/).

1. Introduction

Maraging steels are a class of high-strength steels that provide a good combination of strength and ductility [1]. Therefore they are often used for applications where well-balanced mechanical properties are required. The microstructure of maraging steels consists of a soft lath martensite matrix with high dislocation density, precipitates and sometimes austenite [2]. The mechanical properties of maraging steels are governed by the precipitation of small intermetallic phases and the reversion of martensite to austenite. Both happen during isothermal aging heat treatments at aging temperatures around 400 to 600 °C typically for several hours. The strengthening effect of precipitates was discovered in the early 1900s by A. Wilm [3] and has become a widely used mechanism in modern materials. The precipitates act as obstacles for the movement of dislocations. These obstacles need to be overcome using either the shearing or the bowing (Orowan) mechanism. This increases the shear strength necessary to move the dislocations, leading to a strength increase [4]. Precipitation strengthening depends on many physical properties of the precipitate phase: the coherency with the matrix, the size and distribution, the elastic properties and anti-phase boundary energy [4], to name a few. A model for the strengthening effect, with focus on multi-precipitate systems, was extensively described by Ahmadi et al. [5]. For Co-free, Ti- and Al-alloyed maraging steels the main strength contributing precipitates are the β-NiAl (B2 structure) [6] and the η-Ni_3Ti ($D0_{24}$ structure) phases [7,8]. The β-NiAl precipitates can be identified by their spherical morphology [9,10] and are coherent with the α′-Fe martensitic matrix [11]. β-NiAl is a major strength contributor over a wide range of aging temperatures and aging times due to it's slow coarsening behaviour. This can be attributed to it's small lattice misfit with the matrix [11]. The η-Ni_3Ti precipitates preferably nucleate at dislocations and are only coherent in their early stages. In later aging stages this η-Ni_3Ti phase grows along the dislocation core to form rod-like semi-coherent particles [12].

The reversion of martensite to austenite is strongly dependent and enhanced by the aging temperature, as shown by studies from Nakagawa et al. [13] and Conde et al. [14]. Furthermore, the aging temperature and time have an impact on the location and morphology of the reverted austenite. At the lower end of aging temperatures austenite begins to form as a film-like phase along the lath boundaries, as demonstrated by Zhang et al. [15]. At the higher end of aging temperatures (around 600 °C) block-like austenite can be observed within the martensite matrix [15]. During deformation the reverted austenite is transformed to martensite, this manifests itself as an improvement in ductility and impact toughness (TRIP effect) [16]. For instance: Wang et al. [17] used a strategy based on cold-rolling to achieve a broad grain size distribution of reverted austenite. Using this strategy they could increase the ultimate tensile strength as well as the fracture elongation of a martensitic steel.

Currently, maraging steels are usually aged with isothermal holding followed by air cooling. This can lead to different cooling rates for large and small work pieces or for regions with different thickness within a work piece. The effects of the aging temperature and time are already well studied for many types of maraging steels, but the effect of the cooling rate after holding at the aging temperature is not. The goal of this study is to show how the hardness and the impact toughness of a Co-free Fe-Ni-Cr-Mo-Ti-Al maraging steel are influenced by the cooling rate after the aging heat treatment, with special focus on slow cooling rates. It should also be established how the aging time affects the relationship between the cooling rate and the hardness and impact toughness and how this relationship depends on the microstructural characteristics.

2. Materials and Methods

The material was produced by vacuum induction melting followed by vacuum arc melting for multiple times to ensure a homogeneous ingot. The ingot was then open-die forged to a bar with a diameter of 140 mm. The chemical composition of the maraging steel is displayed in Table 1. After forging the bar was solution annealed at 850 °C for 90 min and quenched in water, followed by a cryogenic treatment at −80 °C for 16 h. The starting point for all aging heat treatment was the solution annealed and quenched condition (SA + Q). Samples with a 12 × 12 mm^2 square profile and a length of 100 mm were cut from the half-radius position of the bar and furnished with a 10 mm deep blind hole with a diameter of 3 mm in the center of the cross section for temperature measurements during aging. The samples were aged at 510 °C with 15 h, 4 h and 0 h aging time. For each aging time 3 samples with constant cooling rates that resulted in cooling times of 56 h, 28 h and 7 h (measured from 510 °C to 100 °C) were produced. The temperature-time profiles of all aging heat treatments are shown in Figure 1. The aging heat treatments were performed in a Nabertherm N11/HR box oven. The core temperature of the samples was measured using a type K thermocouple and tracked using a Eurotherm 6100A data logger. For better readability the aged conditions will be abbreviated using a holding time-cooling time naming system (e.g., 0-56 for 0 h aging time and 56 h cooling time).

The samples for electron backscatter diffraction (EBSD) and X-ray diffraction (XRD) were prepared using standard polishing methods, EBSD samples were finished by electropolishing using a Struers A2 electrolyte. The Vickers hardness was measured using an M4C 025 G3M machine (EMCO-Test, Kuchl, Austria) and a load of 10 kg. The mean hardness and the standard error of mean was calculated using at least five measurements from each condition. The room temperature (21 °C) impact toughness was measured with a Charpy V-notch impact test according to EN ISO148-1 with specimens measuring 55 × 10 × 10 mm^3 and a notch radius of 0.25 mm. One specimen was tested for each condition. The martensite block size was measured with EBSD using a Versa3D DualBeam workstation (FEI, Hillsboro, OR, USA) and an orientation mismatch of 10.5° was used to define the martensite blocks. The austenite fraction was determined by XRD using a Bruker Advanced D8 DaVinci instrument with Cu-Kα radiation and evaluated using LaB_6-calibrated Rietveld refinement.

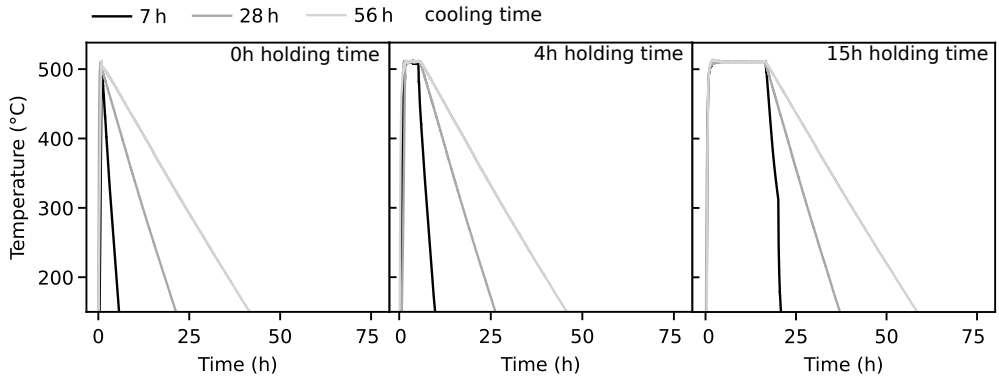

Figure 1. Temperature-time profiles of the aging heat treatments with 0 h, 4 h and 15 h aging time and with 7 h, 28 h and 56 h cooling time.

Table 1. Chemical composition of the maraging steel investigated in this study.

	Fe	Ni	Cr	Mo	Ti	Al	C
wt.%	bal.	12.3	10.2	2.0	1.2	1.5	<0.03
at.%	bal.	11.6	10.8	1.2	1.4	3.1	<0.14

Atom probe tomography (APT) was used to characterize the distribution and chemistry of precipitates. The measurements were performed with a LEAP 3000X HR microscope (Cameca, Gennevilliers Cedex, France) using the laser assisted mode with a pulse frequency of 250 kHz, a laser energy of 0.3 nJ and a detection rate of 1% at a temperature of 60 K. The APT specimens were prepared with a standard 2-step electropolishing method [18]. The first polishing step was performed with a solution of 25 vol% of perchloric acid in glacial acetic acid and the final step was performed with a 2% solution of perchloric acid in 2-butoxyethanol. The IVAS software suite (Cameca, version 3.6.1) was used to analyze the atom probe data. For the statistical evaluation of the precipitates a cluster search based on the maximum separation method was used, upon which the volume fraction F_v of precipitates was calculated according to [19]:

$$F_v = \frac{N \cdot v \cdot C}{V_{total}} \quad (1)$$

N corresponds to the total number of ions found in the clusters corresponding to the precipitates, v to the volume per atom according to the unit cell of the precipitate phase, V_{total} to the total volume of the measurement and C to a correction factor accounting for the detector efficiency. The parameters d_{Max} and N_{Min} used for the maximum separation method are presented in Table 2. d_{Max} is the maximum pair distance between adjacent atoms and N_{Min} minimal cluster size. An order of 4 was used for the maximum separation method. The erosion and envelope distance were chosen to be equal to d_{Max}. The value of d_{Max} was determined using a procedure described by Jägle et al. [20].

The experimental data was used to calculate the contributions of solid solution hardening, grain size hardening, the dislocation density and precipitation hardening to the total hardness. The contribution of the martensite matrix ($\sigma_{\alpha'}$) was determined by using a Hall-Petch model to account for grain size hardening, furthermore the contribution of the dislocation density was also considered within this term. The solid solution strengthening (σ_{SS}) was determined by using the Fleischer model. Both models were implemented as described by Galindo-Nava et al. [21].

$$\sigma_{\alpha'} = \frac{300}{\sqrt{d_{Block}}} + 0.25 M \mu b \sqrt{\rho} \quad (2)$$

$$\sigma_{SS} = \sum_i \left(\beta_i^2 x_i\right)^{1/2} \quad (3)$$

300 MPaμm$^{-1/2}$ is the Hall-Petch constant that was determined for maraging steels [21], d_{Block} is the average martensite block size, μ is the shear modulus of Fe (80.4 GPa [22]), b is the magnitude of the Burgers vector (0.268 nm [21]), ρ is the dislocation density and β_i and x_i are the solid solution factor and the molar fraction of each alloying element. The strength contribution stemming from the dislocation density (σ_ρ) was calculated as the difference between the total strength and the sum of the contributions from solid solution strengthening and grain size strengthening. With the value for σ_ρ the dislocation density was estimated with $\rho = \sigma_\rho^2/(0.25M\mu b)^2$ from Equation (2). The solid solution factor β_i was determined using Equation (4) according to Fleischer's formula [21].

$$\beta_i = \kappa\mu(\eta_i' + 16\delta i)^{3/2} \quad (4)$$

The fitting parameter κ was determined as κ = 0.0045 [21], $\eta_i' = \eta_i/(1 + 0.5\eta_i)$ is calculated from the modulus distortion with respect to pure iron $\eta_i = |\mu_i - \mu_{Fe}|/\mu_{Fe}$ and $\delta_i = |r_i - r_{Fe}|/r_{Fe}$ corresponds to the lattice distortion with respect to pure iron. The shear modulus μ_i and the metallic radius r_i were obtained from [22]. The strength loss due to the formation of reverted austenite was considered using a linear mixture rule as presented by Schnitzer et al. [23] with the strength of 100% pure austenite being σ_γ = 217 MPa. With the volume fractions $F_{\alpha'}$ and F_γ of martensite and austenite respectively, the strength contribution from the matrix can be expressed as: $\sigma_{Matrix} = F_{\alpha'}\sigma_{\alpha'} + F_\gamma\sigma_\gamma$. With this, the yield strength σ_Y of the aged samples can be expressed as:

$$\sigma_Y = \sigma_0 + \sigma_{Matrix} + \sigma_{SS} + \sigma_P \quad (5)$$

σ_0 = 50 MPa corresponds to the strength due to lattice friction [21] and σ_P to the strength contribution due to precipitation hardening. The conversion from the yield strength in MPa to the Vickers hardness value H_V can be performed using a factor 1/3 according to $H_V = \sigma_Y/3$ [24].

Table 2. The central element, maximum pair distance (d_{Max}) and minimal cluster size (N_{Min}) used for the maximum separation method for cluster detection for each condition.

Condition	β-NiAl			η-Ni_3Ti		
	Central Element	d_{Max} (nm)	N_{Min}	Central Element	d_{Max} (nm)	N_{Min}
0-7	Ti	0.95	75			
0-28	Al	0.75	130	Ti	0.95	400
0-56	Al	0.80	150	Ti	0.96	450
4-7	Al	0.78	150	Ti	0.93	800
4-28	Al	0.80	150	Ti	0.98	800
4-56	Al	0.75	130	Ti	0.98	800
15-7	Al	0.70	80	Ti	0.94	700
15-28	Al	0.71	80	Ti	0.94	800
15-56	Al	0.70	140	Ti	0.94	800

3. Results

Figure 2 shows the austenite fractions of all aged conditions. All samples had similar austenite fractions within a range between 7.5% and 12.5%. In the SA + Q condition the austenite fraction was measured and evaluated to be 4.4%. The trend shows an increasing austenite fraction with longer cooling times for the samples with 0 h aging time. For the 4 h and 15 h holding time samples the austenite fraction remained constant within the experimental uncertainty. EBSD revealed that the mean martensite block size was 7.6 μm in the SA + Q condition and between 5.6 μm and 7.6 μm in the aged conditions. No difference

of the matrix microstructure was found between the aged conditions, as shown in Figure 3 for the 0 h aging time samples.

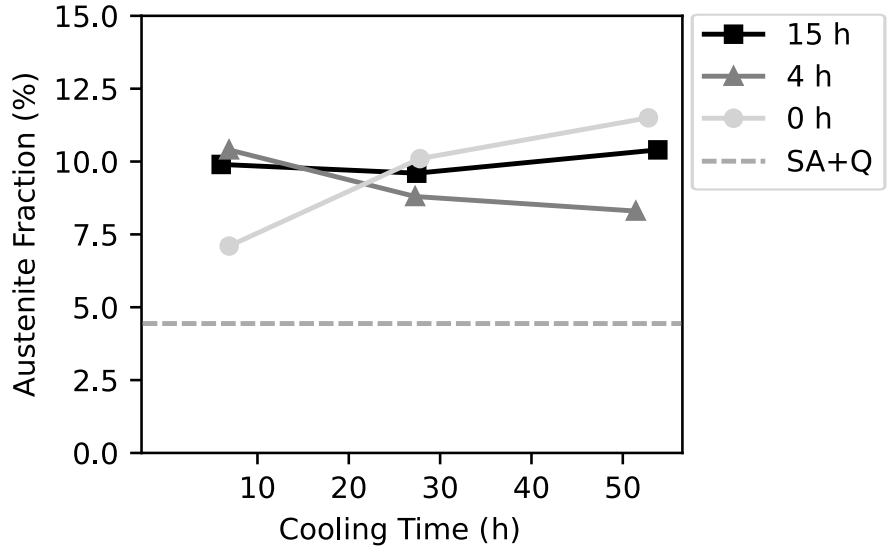

Figure 2. Austenite fraction of the aged conditions with 0 h, 4 h and 15 h aging time as function of the cooling time.

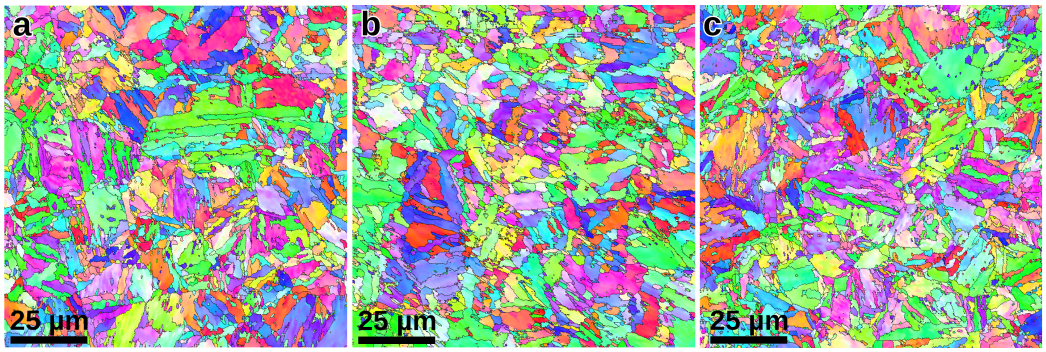

Figure 3. Inverse pole figures obtained from EBSD measurements of the sample group with 0 h aging time and (**a**) 7 h, (**b**) 28 h and (**c**) 56 h cooling time. The martensite block boundaries are represented by lines corresponding to a 10.5° orientation mismatch.

The results from the APT measurements are shown in Figure 4, where the precipitates are represented by iso-concentration surfaces. Two different types of precipitated phases were identified. A spherical phase with approximately equal concentration of Ni and Al, corresponding to a β-NiAl phase, and a rod-like precipitate phase with a Ni to Ti + Al ratio of about 65% Ni and 35% Ti + Al, corresponding to a η-Ni_3(Ti,Al) phase. The size of the η-Ni_3(Ti,Al) phase increased with longer aging time at each cooling time. In the samples with 0 h aging time the η-Ni_3(Ti,Al) phase was only observed in the conditions with 28 h and 56 h cooling time. The η-Ni_3(Ti,Al) phase was found in all conditions of the samples with 4 h and 15 h cooling time.

Figure 5a shows the ratio between Ni and Ti + Al for each heat treatment condition. The Ni to Ti + Al ratio fluctuates around 0.45 for the β-NiAl phase, but for the η-Ni_3(Ti,Al) phase the Ni concentration increases with the aging time. For the 0 h aging time sample the influence of a longer cooling time is displayed by a significantly increased Ni concentration in the η-Ni_3(Ti,Al) phase. The concentration of precipitating elements (Ni, Ti, Al) in the matrix is displayed in Figure 5b. The concentration of Ni, Ti and Al decreased with increasing aging time and partially with increased cooling time.

The volume fraction of each precipitate phase was calculated from the results of the cluster analysis and is shown in Figure 6. For the samples with 0 h and 4 h aging time the volume fraction of the β-NiAl and η-Ni_3(Ti,Al) phases increased between 28 h and 56 h cooling time. For the 15 h aging time sample the volume fraction of η-Ni_3(Ti,Al) decreased with longer cooling times, while the volume fraction of β-NiAl increased with a longer cooling time. The number density of both types of precipitates remained similar for all conditions, with exception of the 4-28 condition where a smaller number density of η-Ni_3(Ti,Al) was observed.

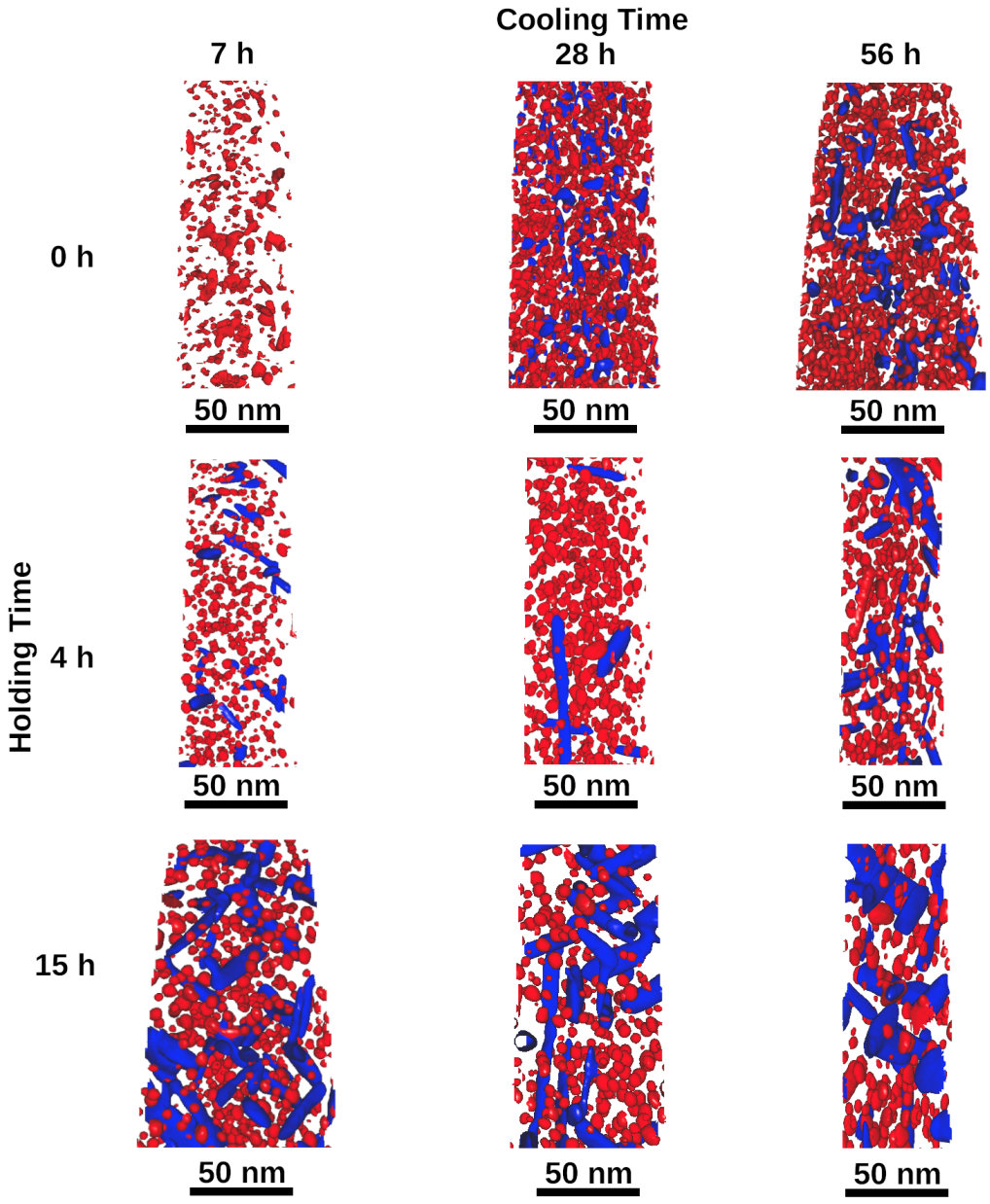

Figure 4. Iso-concentration surfaces showing the precipitate evolution with respect to the cooling time for the 15 h, 4 h and 0 h aged samples. The β-NiAl and η-Ni_3(Ti,Al) phases are represented by 30 at.% Ni + Al (red) and 65 at.% Ni + Ti + Al (blue) iso-concentration surfaces, respectively. For the 0 h aging time samples 25 at.% Ni + Al (red) and 40 at.% Ni + Ti + Al (blue) iso-concentration surfaces are used to represent the η-Ni_3(Ti,Al) and β-NiAl phases, respectively.

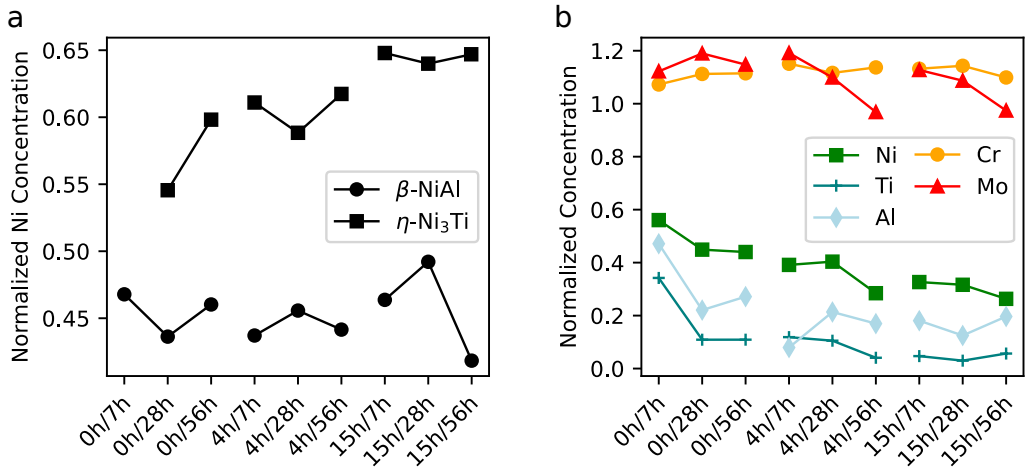

Figure 5. (**a**) Concentration of Ni in the precipitates, normalized to the total concentration of Ni, Ti and Al. (**b**) Concentration of the alloying elements in the matrix phase, normalized to the average bulk composition.

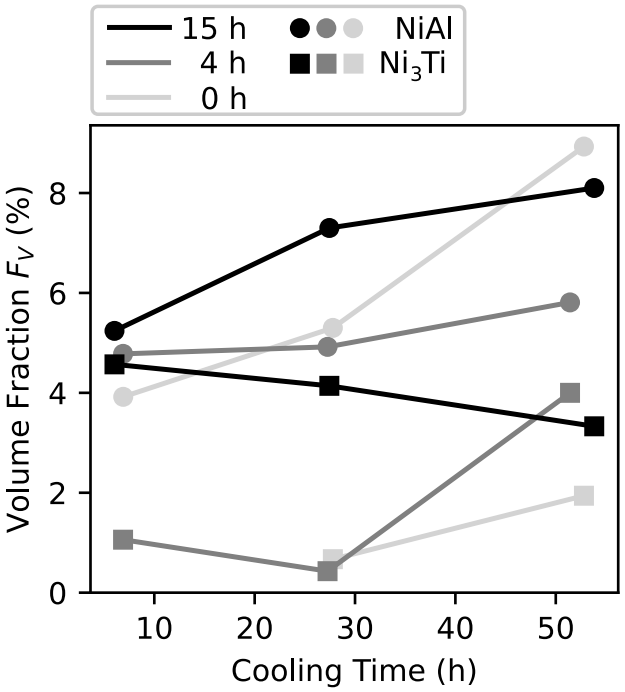

Figure 6. Volume fraction of the precipitates found in the aged conditions as function of the cooling time.

Figure 7a shows that the hardness of the materials increased with increasing cooling time for all 3 aging times. The hardness of the alloy in SA + Q condition was 324 HV10. The increase of hardness with longer cooling time was the strongest in the samples with 0 h aging time and the weakest in the samples with 15 h aging time.

The impact energy for each condition is shown in Figure 7b. No clear correlation was observed for the samples with 15 h and 4 h aging time, however both samples showed a drop in impact toughness for 28 h cooling time. The 0 h sample had a higher impact toughness after long cooling times than after short cooling times.

Figure 8 and Table 3 show the contribution of the matrix, solid solution hardening and precipitation hardening to the total hardness. The 0-7 condition showed the weakest precipitation hardening effect with a value of 296 HV, but the highest contribution from solid solution hardening with a value of 176 HV. Cooling the 0 h aged samples for 28 h or longer led to a significantly increased precipitation hardening effect compared to 7 h cooling

time. The 4 h and 15 h aged samples showed a similar hardening effect due to precipitation hardening after 7 h cooling time. For both aging times the contribution from precipitation hardening increased slightly with longer cooling times, possessing a maximum of 380 HV for the 4-56 condition. The hardness contribution from the matrix was within below 100 HV for all conditions.

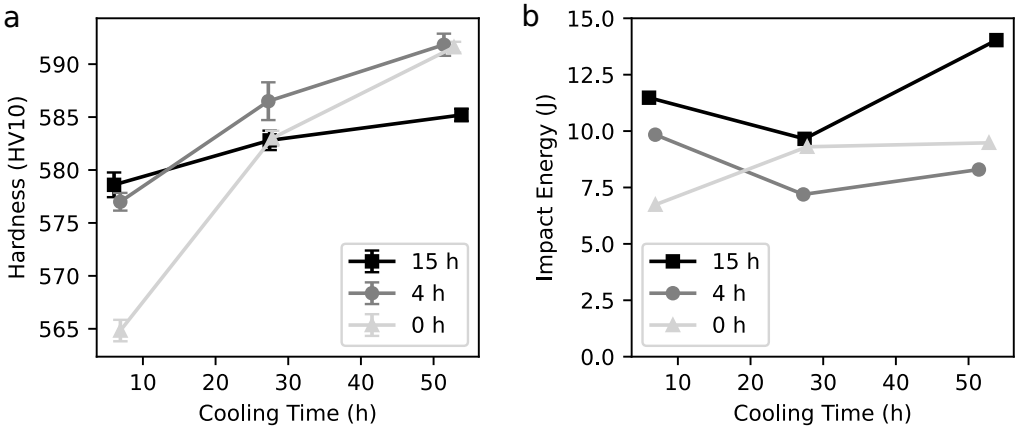

Figure 7. (**a**) Hardness and (**b**) impact toughness of the aged conditions with 0 h, 4 h and 15 h aging time as function of the cooling time.

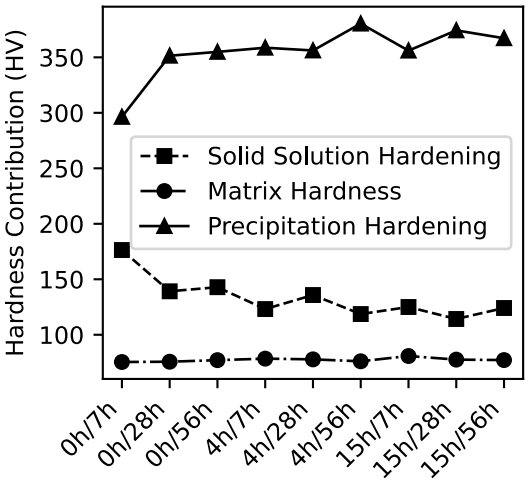

Figure 8. Contributions of different mechanisms to the total hardness for each aged condition.

Table 3. The contribution (in HV) of the matrix ($H_{V,Matrix}$), solid solution hardening ($H_{V,SS}$) and precipitation hardening ($H_{V,P}$) to the total hardness. $H_{V,0}$ corresponds to the hardness due to lattice friction.

Condition	H_V	$H_{V,0}$	$H_{V,Matrix}$	$H_{V,SS}$	$H_{V,P}$
0-7	565	17	75	176	296
0-28	583	17	76	139	351
0-56	592	17	77	143	355
4-7	577	17	78	123	359
4-28	587	17	78	136	356
4-56	592	17	76	119	380
15-7	579	17	81	125	356
15-28	583	17	78	114	374
15-56	585	17	77	124	367

4. Discussion

In this study a Co-free Fe-Ni-Cr-Mo-Ti-Al maraging steel was aged at 510 °C for 0 h, 4 h, and 15 h and cooled using three different cooling rates resulting in a cooling time of 7 h, 28 h and 56 h. Two different types of precipitate phases were identified after aging. The results showed a clear correlation between the cooling time and the hardness, as well as the precipitate evolution.

The changes of the mechanical properties can be discussed purely as an effect of precipitation hardening, austenite reversion and solid solution hardening. This is because the EBSD data showed that no grain growth was observed during aging (Figure 3). Furthermore, all samples were machined from similar positions of the raw material, thus similar degrees of deformation and dislocation density after aging can be assumed.

The austenite fraction remained similar for all cooling times for the 15 h and 4 h aging time samples, while it increased for the samples with an aging time of 0 h. The austenite reversion is directly influenced by the matrix solute content of ferrite (Cr, Mo, Ti, Al) and austenite (Ni) stabilizers and the aging temperature. Various studies [13,14,25,26] show that higher aging temperatures can strongly enhance the austenite reversion kinetics in maraging steels. The results of the 0 h aging time samples show that the austenite reversion and the formation of precipitates occur independent of each other. This is shown by the simultaneously increasing volume fraction of precipitates and austenite, with increasing cooling time. This can be compared to results from Schnitzer et al. [23], where a PH13-8 Mo maraging steel was studied. They found that the formation of austenite in the beginning of aging is independent on the formation of precipitates.

The APT results (Figures 4 and 6) showed that the formation of precipitates is influenced the most by the cooling time for the samples aged for 0 h and 4 h. For a aging time of 15 h both types of precipitates (β-NiAl and η-Ni_3(Ti,Al)) are already well-developed before the cooling process. For this sample group the volume fraction of β-NiAl increases with increasing cooling time, while the volume fraction of η-Ni_3(Ti,Al) decreases. After 4 h of aging only a small volume fraction of η-Ni_3(Ti,Al) is precipitated, when a cooling time of 7 h or 28 h is used. If the cooling time is increased to 56 h, also the 4 h holding sample group showed fully-developed η-Ni_3(Ti,Al) precipitates with volume fractions similar to the 15 h aged sample group. The samples which were immediately cooled after reaching the aging temperature (0 h holding time) showed fully developed precipitates with 28 h and 56 h cooling time. For the 0 h aging time samples, 7 h of cooling time was sufficient to form only clusters and small particles with different morphology and a chemical composition with similar concentrations of Ni and Ti + Al (Figure 5b). From the observed precipitate evolution it can be concluded that the large Ni, Ti and Al rich particles that were observed in this condition correspond to early stages of η-Ni_3(Ti,Al), while the small spherical precipitates correspond to the β-NiAl phase. In addition to the β-NiAl precipitates, the 28 h cooled sample also showed rod-like precipitates with a chemical composition consisting of approximately equal parts of Ni and Ti + Al. This phase can be considered as an incomplete stage of η-Ni_3(Ti,Al). Compared to the samples with 15 h and 4 h aging time the η-Ni_3(Ti,Al) phase is not well-developed in the 0 h aging time samples and the volume fraction is comparatively low. This is because the formation of η-Ni_3(Ti,Al) typically requires longer aging times and forms in a higher temperature range than β-NiAl. In short, a longer cooling time results in a progressing precipitation reaction. If both types of precipitates are fully formed after holding (15 h sample group) the total volume fraction of precipitates remains constant, but a shift from a balanced distribution of η-Ni_3(Ti,Al) and β-NiAl to a distribution with more β-NiAl can be observed.

The results of the hardness testing showed that a clear trend between longer cooling time and an increased hardness exists (Figure 7). Already in the 0-7 condition the hardness increase compared to the SA + Q condition is significant. In this condition, the hardening effect stems from Ni, Ti and Al rich precipitates and clusters with various sizes and morphologies. The increased volume fraction and continued formation of precipitates after longer cooling times (28 h and 56 h) resulted in a hardness increase. Within the 4 h and

15 h sample groups the hardness also was increased by longer cooling times. The results showed that the 0-56 and the 4-56 conditions had the highest hardness out of all samples.

The calculation of the individual contributions to the hardness of the aged alloy showed that the precipitation hardening was within a range of about 350 HV to 380 HV for most conditions (Figure 8). Figure 9 shows the correlation between the volume fraction of precipitates and the precipitation hardening effect. A trend of increased precipitation hardening with a higher volume fraction of precipitates could be observed for all samples and within each aging time group. The strongest precipitation hardening effect was found in the 4-56, 15-28 and 15-56 conditions. This stems from the high volume fraction of precipitates found in these conditions. The weakest contribution of the precipitation hardening to the total hardness was observed for the 0 h aging time sample group. However, due to the comparatively low volume fraction of precipitates a high solute content is present in the matrix. Therefore, a higher contribution from solid solution hardening to the total hardness is present in these conditions. The high hardness that was observed in the 0-56 conditions stems from a well-balanced combination of precipitation hardening and solid solution hardening.

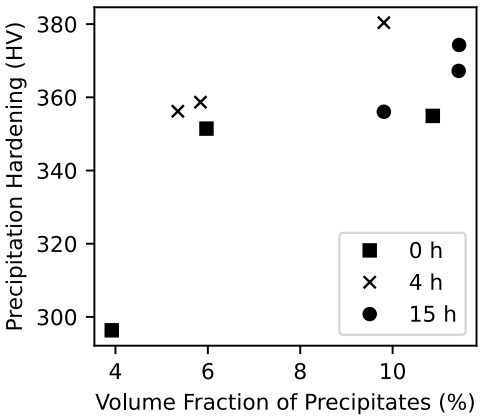

Figure 9. Precipitation hardening as function of the total volume fraction of precipitates (β-NiAl + η-Ni_3(Ti,Al)) for 0 h, 4 h and 15 h aging time.

The hardness contribution from the matrix, including grain size, dislocation hardening and softening due to reverted austenite, remained similar at about 100 HV for all aged conditions. The contribution of the reverted austenite to the matrix hardness was calculated using a linear mixture model, as proposed by Schnitzer et al. [27]. As all aged conditions showed similar austenite fractions, it can be concluded that the reversion from martensite to austenite is not a dominating mechanism for the hardness development of this steel (for an aging temperature of 510 °C).

The results of the Charpy impact tests showed that no correlation between the impact toughness and the cooling rate can be made using the selected heat treatments and experimental conditions. Most conditions showed a similar impact toughness with some fluctuation within each aging time group. No indication of embrittlement, caused by any of the heat treatments, was observed. However, the results suggest that a longer aging time can be beneficial to the impact toughness.

5. Conclusions

Following conclusions can be drawn on the influence of the cooling time on the precipitation hardening effect, impact toughness and microstructural evolution of a Co-free Fe-Ni-Cr-Mo-Ti-Al maraging steel:

- A slow cooling rate can be treated as an extension of the aging heat treatment, that uses lower temperatures. Longer cooling times can result in a higher volume fraction of precipitates and a higher hardness level.

- Solid solution hardening can play an important role for the total strength in under-peak aged precipitation hardened materials and peak hardness can be achieved with early stages of the precipitates.
- The highest hardness of this alloy can be achieved with a long cooling time and without significant loss of impact toughness. There is no clear correlation between the secondary aging effects (austenite reversion and change of impact toughness) and the cooling time.
- Aging heat treatments with a short aging time and long cooling times can be successfully used as an alternative to conventional aging heat treatments. Furthermore, no detrimental effect of long cooling times was found, when longer aging times were used. This knowledge can be useful for large work pieces, where air cooling can result in different cooling rates between the surface and the core of the work piece.

Author Contributions: Data curation, S.Z.; Formal analysis, S.Z.; Investigation, S.Z.; Methodology, S.Z.; Supervision, R.S.; Writing—original draft, S.Z.; Writing—review & editing, R.S. All authors have read and agreed to the published version of the manuscript.

Funding: The authors want to thank the European Research Fund for Coal and Steel (RFCS 847165) for providing the funding that made this study possible. Further thanks goes to the "iNiTiAl" consortium for providing the material.

Data Availability Statement: Access to the experimental data will be given out by the authors upon request.

Conflicts of Interest: The authors declare no conflict of interest.

References

1. Decker, R.F.; Novak, C.J.; Landig, T.W. Developments and projected trends in maraging steels. *JOM* **1967**, *19*, 60–66. [CrossRef]
2. Sha, W.; Guo, Z. *Maraging Steels: Modelling of Microstructure, Properties and Applications*, 1st ed.; Woodhead Publishing Ltd.: Cambridge, UK, 2009.
3. Wilm, A. Physikalisch-metallurgische Untersuchungen über magnesiumhaltige Aluminiumlegierungen. *Metallurgie* **1911**, *8*, 225.
4. Ardell, A.J. Precipitation hardening. *Metall. Trans. A* **1985**, *16*, 2131–2165. [CrossRef]
5. Ahmadi, M.R.; Povoden-Karadeniz, E.; Öksüz, K.I.; Falahati, A.; Kozeschnik, E. A model for precipitation strengthening in multi-particle systems. *Comput. Mater. Sci.* **2014**, *91*, 173–186. [CrossRef]
6. Schober, M.; Schnitzer, R.; Leitner, H. Precipitation evolution in a Ti-free and Ti-containing stainless maraging steel. *Ultramicroscopy* **2009**, *109*, 553–562. [CrossRef]
7. Li, K.; Yu, B.; Misra, R.D.; Han, G.; Liu, S.; Shang, C.J. Strengthening of cobalt-free 19Ni3Mo1.5Ti maraging steel through high-density and low lattice misfit nanoscale precipitates. *Mater. Sci. Eng. A* **2018**, *715*, 174–185. [CrossRef]
8. Leitner, H.; Schober, M.; Schnitzer, R.; Zinner, S. Strengthening behavior of Fe-Cr-Ni-Al-(Ti) maraging steels. *Mater. Sci. Eng. A* **2011**, *528*, 5264–5270. [CrossRef]
9. Schnitzer, R.; Schober, M.; Zinner, S.; Leitner, H. Effect of Cu on the evolution of precipitation in an Fe-Cr-Ni-Al-Ti maraging steel. *Acta Mater.* **2010**, *58*, 3733–3741. [CrossRef]
10. Kürnsteiner, P.; Wilms, M.B.; Weisheit, A.; Barriobero-Vila, P.; Jägle, E.A.; Raabe, D. Massive nanoprecipitation in an Fe-19Ni-xAl maraging steel triggered by the intrinsic heat treatment during laser metal deposition. *Acta Mater.* **2017**, *129*, 52–60. [CrossRef]
11. Jiang, S.; Wang, H.; Wu, Y.; Liu, X.; Chen, H.; Yao, M.; Gault, B.; Ponge, D.; Raabe, D.; Hirata, A.; et al. Ultrastrong steel via minimal lattice misfit and high-density nanoprecipitation. *Nature* **2017**, *544*, 460–464. [CrossRef]
12. Zhang, C.; Wang, C.; Zhang, S.L.; Ding, Y.L.; Ge, Q.L.; Su, J. Effect of aging temperature on the precipitation behavior and mechanical properties of Fe–Cr–Ni maraging stainless steel. *Mater. Sci. Eng. A* **2021**, *806*, 140763. [CrossRef]
13. Nakagawa, H.; Yokota, H.; Miyazaki, T. Effects of aging temperature on the microstructures and mechanical properties of a precipitation hardening martensitic stainless steel containing retained austenite. *J. Mater. Sci.* **2000**, *35*, 2245–2253.[CrossRef]
14. Conde, F.F.; Escobar, J.D.; Oliveira, J.P.; Béreš, M.; Jardini, A.L.; Bose, W.W.; Avila, J.A. Effect of thermal cycling and aging stages on the microstructure and bending strength of a selective laser melted 300-grade maraging steel. *Mater. Sci. Eng. A* **2019**, *758*, 192–201. [CrossRef]
15. Zhang, H.; Ji, X.; Ma, D.; Tong, M.; Wang, T.; Xu, B.; Sun, M.; Li, D. Effect of aging temperature on the austenite reversion and mechanical properties of a Fe-10Cr-10Ni cryogenic maraging steel. *J. Mater. Res. Technol.* **2021**, *11*, 98–111. [CrossRef]
16. Niu, M.C.; Yang, K.; Luan, J.H.; Wang, W.; Jiao, Z.B. Cu-assisted austenite reversion and enhanced TRIP effect in maraging stainless steels. *J. Mater. Sci. Technol.* **2022**, *104*, 52–58. [CrossRef]
17. Wang, M.; Tasan, C.C.; Ponge, D.; Raabe, D. Spectral TRIP enables ductile 1.1 GPa martensite. *Acta Mater.* **2016**, *111*, 262–272. [CrossRef]

18. Gault, B.; Moody, M.; Cairney, J.M.; Ringer, S.P. *Atom Probe Microscopy*; Springer: New York, NY, USA, 2012.
19. Zeisl, S.; Lassnig, A.; Hohenwarter, A.; Mendez-Martin, F. Precipitation behaviour of a Co-free Fe-Ni-Cr-Mo-Ti-Al maraging steel after severe plastic deformation. *Mater. Sci. Eng. A* **2021**, *833*, 142416. [CrossRef]
20. Jägle, E.A.; Choi, P.P.; Raabe, D. The maximum separation cluster analysis algorithm for atom-probe tomography: Parameter determination and accuracy. *Microsc. Microanal.* **2014**, *20*, 1662–1671. [CrossRef]
21. Galindo-Nava, E.I.; Rivera-Díaz-Del-Castillo, P.E. A model for the microstructure behaviour and strength evolution in lath martensite. *Acta Mater.* **2015**, *98*, 81–93. [CrossRef]
22. Warlimont, H.; Martienssen, W. *Springer Handbooks of Materials Data*, 2nd ed.; Springer Nature: Cham, Switzerland, 2018.
23. Schnitzer, R.; Radis, R.; Nöhrer, M.; Schober, M.; Hochfellner, R.; Zinner, S.; Povoden-Karadeniz, E.; Kozeschnik, E.; Leitner, H. Reverted austenite in PH 13-8 Mo maraging steels. *Mater. Chem. Phys.* **2010**, *122*, 138–145. [CrossRef]
24. Galindo-Nava, E.I.; Rainforth, W.M.; Rivera-Díaz-del Castillo, P.E. Predicting microstructure and strength of maraging steels: Elemental optimisation. *Acta Mater.* **2016**, *117*, 270–285. [CrossRef]
25. Escobar, J.D.; Faria, G.A.; Wu, L.; Oliveira, J.P.; Mei, P.R.; Ramirez, A.J. Austenite reversion kinetics and stability during tempering of a Ti-stabilized supermartensitic stainless steel: Correlative in situ synchrotron X-ray diffraction and dilatometry. *Acta Mater.* **2017**, *138*, 92–99. [CrossRef]
26. Kooiker, H.; Perdahcıoğlu, E.S.; van den Boogaard, A.H. Combined athermal and isothermal martensite to austenite reversion kinetics, experiment and modelling. *Mater. Des.* **2020**, *196*, 109124. [CrossRef]
27. Schnitzer, R.; Zickler, G.A.; Lach, E.; Clemens, H.; Zinner, S.; Lippmann, T.; Leitner, H. Influence of reverted austenite on static and dynamic mechanical properties of a PH 13-8 Mo maraging steel. *Mater. Sci. Eng. A* **2010**, *527*, 2065–2070. [CrossRef]